Title

CALCULATION OF THE BAND STRUCTURE AND OPTICAL CONSTANTS OF DIAMOND USING THE NON-LOCAL PSEUDOPOTENTIAL METHOD

Authors

Hemstreet, Louis A.
Fong, C.Y.
Cohen, Marvin L.

Publication Date

1970-03-01

Submitted to Physical Review

UCRL-19197
Preprint

c. 2

CALCULATION OF THE BAND STRUCTURE AND OPTICAL CONSTANTS OF DIAMOND USING THE NON-LOCAL PSEUDOPOTENTIAL METHOD

Louis A. Hemstreet, Jr., C. Y. Fong, and Marvin L. Cohen

March 1970

AEC Contract No. W-7405-eng-48

LAWRENCE RADIATION LABORATORY
UNIVERSITY of CALIFORNIA BERKELEY

DISCLAIMER

Calculation of the Band Structure and Optical Constants of Diamond Using the Non-local Pseudopotential Method

Louis A. Hemstreet, Jr.
Department of Physics, University of California
Davis, California 95616

C. Y. Fong
Inorganic Materials Research Division
Lawrence Radiation Laboratory
University of California
Berkeley, California 94720
Department of Physics, University of California*
Davis, California 95616

Marvin L. Cohen†**
Department of Physics
and Inorganic Materials
Research Division,
Lawrence Radiation Laboratory
University of California, Berkeley, California 94720

† Professor, Miller Institute for Basic Research in Science 1969-70

** Supported in part by the National Science Foundation

* Present Address

Abstract

The electronic band structure and optical constants of diamond are calculated using the empirical pseudopotential method with an additional ℓ=1 non-local term $V_{NL}(\vec{r})$ added to account for the strong potential experienced by p-electrons in the core region. $V_{NL}(\vec{r})$ strongly effects the p-like conduction bands, and the resulting band structure yields a plot of $\epsilon_2(\omega)$, the imaginary part of the dielectric function, which is in satisfactory agreement with experiment. In addition, the temperature-dependent peak at 7.8 eV in the optical spectrum, whose origin has been somewhat of a mystery, is identified with optical transitions beginning at L and extending out along the Λ direction in the B.Z..

Introduction

The band structure of diamond has been extensively studied by several authors[1-5] in recent years. We will focus here on those calculations utilizing the empirical pseudopotential method[1-3] (EPM) with the aim of extending these calculations. Since good pseudopotential calculations for silicon are presently available in the literature[6], it would seem to be possible to combine the best sets of form factors for C and Si to determine a consistent band structure for SiC. Furthermore, the form factors for C can be used to determine the symmetric part of the form factors for BN and BP. However, before proceeding directly toward these goals, further improvement on the presently available diamond calculations is considered necessary as the resulting band structures do not yield a totally satisfactory fit to the experimental optical data. In particular, the calculated ε_2 spectra of diamond do not match the measured spectra very well[3], especially with respect to the line shape in the low energy region and the position of the main peak.

In an attempt to correct for the above deficiencies, we present in this paper another calculation of the band structure and optical properties of diamond. However, instead of making the usual assumption that the pseudopotential can be approximated by a local, spherically-symmetric potential which is independent of the angular momentum of the state under consideration, we have included a non-local term $V_{NL}(\vec{r})$ to account for the angular-momentum dependence of the pseudopotential. Such a term does indeed lead to an improved line shape in the low energy region, and yields a main peak whose position is in excellent agreement with experiment. In addition, the band structure thus obtained suggests a new interpretation of some of the optical structure. In what follows, we shall describe more fully the details and results of these calculations. The paper will be presented in three sections: section I

discusses the choice of $V_{NL}(\vec{r})$, and briefly describes the mechanics of the calculation; section II discusses the resulting energy band structure and optical parameters, comparing them to the results of other authors; finally, section III presents conclusions drawn from the calculation.

I. Non-Local Analysis

In the original formulation of the pseudopotential method, as described by Phillips & Kleinman[7], instead of solving the one-electron Schrödinger equation for a periodic crystal,

$$\left[\frac{p^2}{2m} + V(\underset{\sim}{r}) \right] \psi_{n\underset{\sim}{k}}(\underset{\sim}{r}) = E_n(\underset{\sim}{k}) \psi_{n\underset{\sim}{k}}(\underset{\sim}{r}) \tag{1}$$

where p and m are the momentum and mass of the electron and $V(\vec{r})$ is the crystal potential, one considers instead the following model equation for a smoothed pseudo-wavefunction $\phi_{n\underset{\sim}{k}}(\vec{\underset{\sim}{r}})$:

$$\left[\frac{p^2}{2m} + V_p(\underset{\sim}{r}) \right] \phi_{n\underset{\sim}{k}}(\underset{\sim}{r}) = E_n(\underset{\sim}{k}) \phi_{n\underset{\sim}{k}}(\underset{\sim}{r}) \tag{2}$$

where V_p is a nonlocal integral operator representing the sum of the usual attractive Coulomb crystal potential, V_c, and a non-local, angular-momentum-dependent repulsive potential, V_R, which arises from the orthogonality of the true wavefunctions to the core states.

In order to solve equation (2), the usual procedure is to assume the cancellation between V_R and V_C to be almost complete, and to replace V_p by a weak potential which is independent of angular momentum. In addition, one generally approximates the pseudopotential by a local, spherically symmetric potential, which is assumed to be expressible as a superposition of local, spherically symmetric potentials centered about each ion site. With these approximations, one can then write

$$V_p(\underset{\sim}{r}) = \sum_j v(|\underset{\sim}{r} - \underset{\sim}{R}_j|) \tag{3}$$

where $v(|\underset{\sim}{r}-\underset{\sim}{R}_j|)$ is the local potential centered at $\underset{\sim}{R}_j$, the position of the jth ion core, and the sum is over all the ion cores in the crystal. The problem of determining the energy eigenvalues and pseudo-wavefunctions is

thus reduced to solving the somewhat simpler equation

$$\left[\frac{p^2}{2m} + \sum_j v(|\underset{\sim}{r} - \underset{\sim}{R}_j|) \right] \phi_{n\underset{\sim}{k}}(\underset{\sim}{r}) = E_n(\underset{\sim}{k}) \phi_{n\underset{\sim}{k}}(\underset{\sim}{r}) \tag{4}$$

for the various cases of interest.

It is from this point that previous EPM calculations have proceeded. However, in the case of diamond, the agreement between the results of such calculations and the experimental optical data is not particularly good[3]. This is somewhat surprising, since eq. (4) leads to good results for Ge and Si, which have essentially the same structure. This suggests that the approximations leading to equation (4) should be re-examined for diamond. In particular, the approximation involved in ignoring the angular momentum dependence of V_p seems somewhat questionable. Unlike Si and Ge, diamond has no p electrons in the core; hence, the Coulomb potential felt by the p valence and conduction electrons is not cancelled in the core region by a repulsive term from V_R. As a result, Phillips Cancellation Theorem[8] is not valid in this case, and one cannot assume V_p to be weak in this region for such electrons. In light of this fact, we modify eq. (4) in our calculation by adding to it a non-local term, $V_{NL}(\vec{r})$, to account for the strong potential experienced by p states in the core. Thus, instead of using equation (4) as a starting point for our calculation, we use the following equation:

$$\left[\frac{p^2}{2m} + \sum_j v(|\underset{\sim}{r} - \underset{\sim}{R}_j|) + V_{NL}(\underset{\sim}{r}) \right] \phi_{n\underset{\sim}{k}}(\underset{\sim}{r}) = E_{n\underset{\sim}{k}} \phi_{n\underset{\sim}{k}}(\underset{\sim}{r}) \tag{5}$$

where $V_{NL}(\underset{\sim}{r})$ is assumed to operate only on p states in the core region. To satisfy these conditions, we have followed the analysis of Lee & Falicov[9] for K and Fong and Cohen[10] in their treatment of KCl by choosing $V_{NL}(r)$ to have the form

$$V_{NL}(\underset{\sim}{r}) = \sum_j \hat{P}_1^{+} \, v(|\underset{\sim}{r} - \underset{\sim}{R}_j|) \, \hat{P}_1 \tag{6}$$

where $\hat{P}_1$ is a projection operator which operates only on those spherical harmonics with $\ell=1$, and P_1^+ is the corresponding hermitean conjugate operator.

During the course of the calculation, several forms of $U(|\underline{r}|)$ were tried, such as a simple square well, a Yukawa-type well, etc. The best results are obtained by choosing

$$U(|\underline{r}|) = \begin{cases} Are^{-\alpha r}, & r \le R_s \\ 0, & r > R_s \end{cases} \tag{7}$$

where R_s is the diamond core radius in the crystal, assumed to retain its free atom value of approximately 0.2Å, and A and α are treated as parameters. This choice of $U(|\underline{r}|)$ is vaguely suggestive of the Coulomb potential (proportional to $\frac{1}{r}$) felt by an atomic p-electron, which has an associated radial charge density of the form $r^2e^{-\alpha r}$, in the presence of a point nucleus. The calculation resulting from this choice of U will be the only one discussed in this paper.

To solve (5), it is convenient to expand the weak local pseudopotential term in the reciprocal lattice as follows:

$$\sum_j v(|\underline{r}-\underline{R}_j|) = \sum_{|\underline{G}|^2 \le 12} v(|\underline{G}|) S(|\underline{G}|) e^{i\underline{G}\cdot\underline{r}} \tag{8}$$

where $\underline{G}$ is a reciprocal lattice vector in units of $2\pi/a$, a is the lattice constant of diamond, taken to be the value 3.57Å,

$$v(|\underline{G}|) = \frac{2}{\Omega} \int_{\text{cell}} v(|\underline{r}|) e^{-i\underline{G}\cdot\underline{r}} \, d^3r \tag{9}$$

is the crystal form factor, Ω is the volume of the unit cell, and

$$S(|\underline{G}|) = \cos \underline{G}\cdot\underline{\tau} \tag{10}$$

is the structure factor, $\tau = \frac{a}{8}(1,1,1)$ being the vector between the two

diamond atoms in the unit cell. With the truncation of the expansion at $|\underline{G}^2|=12$ in (8), the only non-vanishing form factors are $v(|G|^2=3)$, $v(4)$, $v(8)$, $v(11)$, and $v(12)$. $v(4)$ and $v(12)$ do not contribute to the potential because the corresponding structure factors $S(4)$ and $S(12)$ are zero. However, we set $S(12)=1$ in order to be consistent with the x-ray scattering data[11,12].

Having made the expansion (8), one then diagonalizes the pseudopotential Hamiltonian (5) over a basis of plane wave states. The matrix elements for the local pseudopotential are calculated by a method described by Brust[13]. Essentially, this method consists of treating those plane waves satisfying $|\underline{k}+\underline{G}|^2 \leq E_1$ exactly, while those with $E_1 < |\underline{k}+\underline{G}|^2 \leq E_2$ enter only through second order pertubation theory. Plane waves with $|\underline{k}+\underline{G}|^2 > E_2$ are neglected. For the non-local term $V_{NL}(r)$ we also neglect the contributions of those plane waves with $E_1 < |\underline{k}+\underline{G}|^2 < E_2$. A typical matrix element of V_{NL} is of the form

$$\langle \underset{\sim}{k}+\underset{\sim}{G} | V_{NL} | \underset{\sim}{k}+\underset{\sim}{G}' \rangle = I_{\underset{\sim}{G}\underset{\sim}{G}'} \frac{24}{\Omega} \cos\theta_{\underset{\sim}{G}\underset{\sim}{G}'} S(\underline{G}-\underline{G}') \quad , \tag{11}$$

where

$$I_{\underset{\sim}{G}\underset{\sim}{G}'} = \int j_1(|\underset{\sim}{k}+\underline{G}|r)\, j_1(|\underset{\sim}{k}+\underline{G}'|r)\, U(r)\, r^2\, dr \quad , \tag{12}$$

j_1 is the spherical Bersel function of order 1, $\theta_{\underline{GG}'}$ is the angle between the vectors $\underline{k}+\underline{G}$ and $\underline{k}+\underline{G}'$, and Ω and S are the volume of the unit cell and structure factor as defined previously. The integral is evaluated numerically. Satisfactory convergence is obtained by choosing $E_1=12.50$ and $E_2=30.10$.

The EPM method of solution of (5) consists in choosing the pseudopotential form factors $v(\underline{G}_j)$, along with the parameters A,α associated with $U(r)$, to give band structures consistent with experiment. In practice, one calculates a few of the principal band gaps at important symmetry points in

the Brillouin zone, and then adjusts these parameters until the gap values agree with those extrapolated from the optical experimental data. Once these parameters are fixed, the energies can be calculated at general points throughout the zone. The resulting band structure and pseudo-wavefunctions can then be used to calculate ε_2 via the expression

$$\epsilon_2(\omega) = \frac{e^2\hbar^2}{m} \sum_{v,c} \frac{2}{(2\pi)^3} \int \frac{f_{vc}(\underset{\sim}{k})\, dS}{E_{vc} |\nabla_{\underset{\sim}{k}} E_{vc}|} \tag{13}$$

where

$$f_{vc}(\underset{\sim}{k}) = \frac{2}{3m} \frac{|\langle \underset{\sim}{k}, v | \underset{\sim}{p} | \underset{\sim}{k}, c \rangle|^2}{E_{vc}}$$

is the EPM interband oscillator strength, $|k,c\rangle$ and $|k,v\rangle$ are the EPM wavefunctions for the conduction and valence bands at the point $\underline{k}$, S is a surface of constant interband energy $E_{vc} = E_c - E_v$, and E_c and E_v are the energies of the conduction and valence bands, respectively. The details of evaluating the sums over initial and final states is described elsewhere[14]. The only modifications are that the mesh size is defined by dividing the distance ΓX into ten parts, each cube is divided into 125 equal subcubes, yielding ~13,600 random points, and quadratic interpolation between mesh points is used instead of linear interpolation. The whole process is repeated until satisfactory agreement with the optical data is obtained or until no further improvement can be obtained.

The available optical data for diamond can be summarized by a plot of ε_2[16], as shown by the dashed line in Fig. 2. We also list the measured values of the conduction band minimum, Δmin, and the threshold for indirect transitions E_{ind}[17,18] (see Table II). As can be seen, the experimental ε_2 has

structure at 7.2, 7.8, 12, and 16 eV. Presumably, these structures can be related to Van Hove singularities at critical points, where $\nabla_{\underline{k}} E_{vc} = 0$, although it is possible that they may also arise from transitions extending over large regions of k space around symmetry points, as Kane showed to be the case for Si[19]. It is by identifying the structure with transitions at certain critical symmetry points that one determines the data to which the form factors are fit.

Unfortunately, no clear cut interpretations of the critical points causing the principal structure in the low energy region of the diamond ε_2 spectrum exist. The shoulder at 7.2 eV is temperature independent[16], which suggests that the threshold for direct transitions is near this energy. However, there is some debate as to whether this fundamental absorption edge begins with transitions at Γ or L^3. The peak at 7.8 eV is temperature dependent, which suggests the possibility of its being caused by an exciton; however, previous calculations yield no critical point near this energy with which such an exciton can be associated. By contrast, the origin of the main peak at 12 eV is understood to arise from 4→5 transitions starting at X ($X_4 \rightarrow X_1$) and extending out along the Σ directions, where there is a large region of essentially parallel bands. The structure at 16 eV is not sharp and is at too high an energy to be given accurately by our EPM approximation.

For the purposes of this calculation, then, the only unambiguous experimental data to which the form factors can be fit are the threshold for indirect transitions, the position of the conduction band minimum, and the position of the main peak, which is expected to lie near the $X_4 \rightarrow X_1$ transition energy. The experimental values taken for these quantities are listed in Table II, under experiment. In addition, we assume that the threshold for direct transitions occurs at Γ with energy in the vicinity of 7 eV. Since

prior calculations agree fairly well with all of the above data but the position of the main peak, we have directed our efforts towards improving this value. As a starting point in our calculation, we use the local form factors V_{111}, V_{220}, V_{311}, V_{222} of Saslow[1] et. al. (Table I). They are combined with A,α and adjusted until satisfactory agreement with the optical data is reached.

II. Discussion of Results

The resulting pseudopotential form factors, principal energy gaps, and positions of Δmin and the main peak are given in tables I and II. For convenience results of other recent calculations are also listed. The calculated energy band structure along principal symmetry lines is shown in Fig. 1. Fig. 2 contains the calculated $\varepsilon_2(\omega)$ spectrum for the range 0-20 eV, with the corresponding experimentally-derived curve also included for comparison. The theoretical reflectance $R(\omega)$, obtained via a Kramers-Kronig analysis of our calculated ε_2 using the method of Walter and Cohen[15], is shown in Fig. 3, accompanied by the measured curve. Finally, Figs. 4,5 indicate important energy contours and critical points for 4→5 and 4→6 transitions, respectively.

We will first consider the calculated band structure. The valence band maximum is at Γ, and the conduction band minimum occurs near (.80,0,0), which is in good agreement with the value of (.78 ± .02,0,0) determined via neutron diffraction studies[17]. The threshold for indirect transitions is seen to be 5.46 eV[17,18], in excellent agreement with experiment. The threshold for direct transitions is 6.96 eV, and corresponds to $\Gamma_{25'}\rightarrow\Gamma_{2'}$ transitions. The band structure is similar in most respects to those of prior calculations, including the APW calculations of Keown[4] and Herman's OPW calculation[5]. However, there are some significant differences, mainly with respect to the level ordering at Γ and L. The present calculation has $\Gamma_{2'}$ lower than Γ_{15}, which agrees with Saravia & Brust[3], but is opposite to the ordering of other calculations. A priori, there is no reason for choosing one ordering over the other. One might argue that, since Ge and Sn have $\Gamma_{2'}$ lower than Γ_{15}, while Si has the order reversed, C could be expected to follow the trend and have Γ_{15} lower in energy than $\Gamma_{2'}$. However, there is no experimental data presently available which favors one ordering over the other. Until such time

as experiments can isolate some effect which differentiates between the two, the question of which ordering is correct remains open. Another difference in the levels occurs at L, where L_2' is lower in energy than L_1, L_3, and Γ_2, and L_1 and L_3, are reversed, with L_3 lower than L_1. The fact that L_2' lies lower than L_1, L_3 is related to the fact that Γ_2' lies below Γ_{15}. The peak which appears at 8.4 eV in the calculated reflectance spectrum (Fig. 3) is a consequence of the fact that the conduction band at L (L_2') has been brought down closer to the valence band.

The calculated ε_2 spectrum begins with direct 4→5 transitions at Γ with energy 6.96 eV. As just discussed, this corresponds to the $\Gamma_{25}'\rightarrow\Gamma_2'$ transition, which has M_0 symmetry. Since the contributions to ε_2 near 7 eV come from a very small region in $\underline{k}$-space, as shown in Fig. 4, the absorption edge is very weak in this vicinity and does not show up well on the curve. As the energy is increased, more and more states are able to contribute and ε_2 starts to rise. The slope in the region 7.5-8 eV is quite steep because the joint density of states with transition energies in this range increases quite rapidly, as indicated by the much larger energy contour for 8.1 eV in Fig. 4a, and the associated oscillator strengths are very large, especially out along the Λ and Σ directions from Γ. At 8 eV, the curve starts to level off somewhat, as the increase in J_{vc}, the joint density of states, is not quite as rapid as before; in addition, much of the increase in J_{vc} comes from interior points in the zone in a region where the oscillator strengths are generally weaker than before.

Near 8.2 eV, ε_2 again changes slope and begins another steep ascent until $\hbar\omega$ = 8.4 eV, where it starts to level off again. In this region there are three main contributions to ε_2. First, there is an M_0 singularity at Γ, corresponding to the (4→6) transition $\Gamma_{25}'\rightarrow\Gamma_{15}$ with energy 8.2 eV. In addition,

there is a second critical point at L which has M_1 symmetry and is associated with the (4→5) transition $L_{3'} \rightarrow L_{2'}$ of energy 8.27 eV. Finally, there is a large increase in J_{vc} in this energy interval coming mostly from 4→5 transitions in the region around L and extending out along Λ, where the oscillator strengths are fairly large.

The structure exhibited by ε_2 from 8.4 to 11.5 eV is not associated with any critical points but seems to be solely due to a volume effect. The major contributions come from 4→5 transitions in the interior of the zone, as shown in Fig. 4 for selected energies; 4→6 transitions around Γ also contribute, but not significantly, as the available phase space is of limited extent, and the oscillator strengths are generally weaker. The roughness in the region 8.4-10 eV arises primarily because of the sampling procedure used in evaluating the sums over initial and final states in (13). In this range, the energies change quite rapidly with position in the B.Z. As a result, the meshes used to divide up the Brillouin zone when performing the sums are probably too coarse to yield accurate energy levels and EPM oscillator strengths at random $\underline{k}$ values in this region. Previous experience indicates that dividing the BZ into a finer mesh should smooth out the curve in this region. This belief is strengthened by the fact that the calculated reflectance (Fig. 3) is absolutely smooth in this range. In the interval 10-11.5 eV, the major contribution to ε_2 comes from 4→5 transitions in the interior of the zone, coming closer to the region around K,U,X as the energy increases. The steep rise in ε_2 is due to the fact that the oscillator strengths become significantly stronger as one goes away from Γ, L and toward the region around K,U,X.

The large main peak at 11.8 eV is caused by the M_1 critical point at X with energy 11.79 eV, corresponding to the (4→5) transition $X_4 \rightarrow X_1$. The main contribution still comes from 4→5 transitions, especially those in the XΓKW

plane as shown in Fig. 4b. (3→5) and (4→6) transitions also combine in roughly equal proportions to make up about 10% of the total contribution to ε_2 at this point.

As one goes higher in energy, the 4→6 transitions become more and more important. Since the oscillator strengths are generally much weaker than those corresponding to the 4→5 transitions, ε_2 falls smoothly as energy increases. The peak at 13.2 eV is due to the M_1 critical point at L associated with the (4→6) transition $L_{3'}\rightarrow L_3$ with energy 13.13 eV. The small peak at 14.4 eV is caused by the (4→6) transition $\Delta_5\rightarrow\Delta_{2'}$ at the point (0.5 ,0,0); this transition has energy 14.38 eV and M_2 symmetry.

A comparison with the experimentally derived ε_2 yields generally adequate agreement. The main purpose of this calculation is to try to improve the agreement between the position of the main peak in the theoretical and experimental results. In previous calculations[3], the calculated position of the main peak is displaced from its experimental value by ∿1 eV. As seen from Fig. 2, in this calculation the two peaks are in excellent agreement, differing in position by only 0.2 eV. The calculated peak is somewhat larger in magnitude but this seems to be characteristic of the EPM-type calculations. The height of the experimental ε_2 curve is somewhat arbitrary, anyway, as surface contamination of the sample can lead to differences in peak height of up to 20%[15] in the measured reflectance, from which ε_2 is derived. Since the measured and calculated peak heights for the reflectance differ by only 5% or so, as shown in Fig. 3, one can assume that the magnitude differences in ε_2 are probably due to the different methods employed in evaluating the Kramers-Kronig integrals in the higher energy regions; we used an analytic tail of the form $\beta\omega/(\omega^2+\gamma^2)^2$ to replace the calculated $\varepsilon_2(\omega)$ for energies above 24 eV, while Walker used Roesslers' method[19] to extend his values of $R(\omega)$ beyond the

measured range 5-31 eV (see refs. 15,16 for a more detailed comparison of the methods). The difference in magnitudes of the two ε_2, along with the different extrapolation methods used, should also explain why the positions of the main peak are displaced further apart in $R(\omega)$ ($\sim$.4 eV) than in ε_2. Any altering of the peak heights in $R(\omega)$ (or ε_2) would be expected to cause energy shifts when transforming to $\varepsilon_2(\omega)$ (or R).

The agreement between theory and experiment in the 7-10 eV region is not extremely good, but this range has always been a troublesome one for theorists. As remarked earlier, the cause of the experimental structure between 7-8 eV is very uncertain. The calculated ε_2 starts off with a slope very similar to that of the measured curve, but displaced approximately 0.8 eV higher in energy. The shape of this absorption edge is much improved over that obtained by Saravia and Brust[3], using Saslow's form factors, which is much too weak compared to experiment. Saravia and Brust do calculate a strong absorption edge near 7.3 eV, with their model II[3], but the slope is too steep, being almost vertical and essentially forming a step function. Neither calculation accounts for the peak at 7.8 eV. A close look at Fig. 2 shows two "bends" in the calculated ε_2 at 8.1 and 8.3 eV. This structure shows up more prominently in $R(\omega)$ (fig. 3), where there are two small peaks at 8.3 and 8.6 eV. These seem to correspond to the measured peaks at 7.2 and 7.6, but are displaced in energy by $\sim$1 eV. Since these calculated peaks are caused by the M_0 and M_1 critical points at Γ and L respectively, it seems likely that their positions could be shifted down in energy by reducing the energy gaps between $\Gamma_{25'}$ and Γ_{15} at Γ, and between $L_{3'}$ and $L_{2'}$ at L. Unfortunately, this turns out to be very difficult with our model potential for u(r). It was found that decreasing the $L_{3'} \rightarrow L_{2'}$ gap at L could only be accomplished by lowering the conduction band, the valence band remaining essentially unchanged. However, any significant lowering of the conduction band at L has the effect of shifting

the conduction band minimum from Δmin to L_2'. Thus, any shifting of the gap at L must be done by shifting the valence band upward.

The gap at Γ, corresponding to the $\Gamma_{25'} \rightarrow \Gamma_{15}$ transition, can be handled much more easily. However, as long as L is kept near 8.2 eV in energy, the agreement with experiment of the overall line shape in the low energy range deteriorates, with the absorption edge becoming weaker as Γ_{15} is lowered. This indicates that one must lower both Γ and L at the same time, as the slope of the experimental ϵ_2 curve in the low energy region seems to depend on the two gaps being close together in energy. At this time, we have not been able to accomplish the raising of the point L_3', the valence band at L. However, we tentatively associate the peak at 7.2 in the experimental ϵ_2 with the M_0 critical point at Γ, corresponding to the $\Gamma_{25'} \rightarrow \Gamma_{15}$ transition, and the peak at 7.8 eV with the $L_3' \rightarrow L_2'$ transition at L, which has M_1 symmetry. This is the first theoretical identification of a critical point associated with the peak at 7.8 eV. The association of the peak at 7.2 with the $\Gamma_{25'} \rightarrow \Gamma_{15}$ transition is not new, but agrees with the identification made by Herman et.al.[5] and Saslow et.al.[1] However, in our case, we do not also assume that $\Gamma_{25'} \rightarrow \Gamma_{15}$ forms the threshold for direct transitions, but instead delegate this honor to the $\Gamma_{25'} \rightarrow \Gamma_2'$ transition occuring near 7 eV.

In the region 8.5 to 10 eV, the calculated ϵ_2 is too strong and too rough. The roughness probably arises from sampling techniques, as discussed previously, and disappears altogether in the reflectance (Fig. 3), which is very smooth in this region; the magnitude of the curve is still larger than the experiment in this region. From 10-13 eV the two ϵ_2 plots agree quite well, except for the magnitude of the main peak. The slopes of the two curves are quite similar in this region. From 13 eV up, the calculated curve is again larger than experiment, and has peaks at 13.2 and 14.4 eV which don't show up in the experimental curve.

III Conclusions

As discussed in the previous section, the non-local EPM calculation seems to explain most of the observed structure in the dielectric constant $\epsilon_2(\omega)$ and the reflectance $R(\omega)$ for diamond, at least qualitatively. The calculation indicates that the experimental peaks in ϵ_2 and R near 8 eV can be associated with the M_1 critical point at L, even though the calculated value of the $L_3' \rightarrow L_2'$ energy gap seems to be ~0.5 eV too large; the temperature dependence of the experimental peak could be caused by an exciton associated with this point. The position of the main peak has been brought into excellent agreement with experiment. Calculations done without $V_{NL}(r)$ indicate that the non-local potential has a definite effect on states within the zone as well as on those along symmetry lines. An illustration of this effect is the significant shift introduced in the position of the main peak, which has large contributions from extended regions in $\underline{k}$-space. Further improvement in the quantitative agreement between theory and experiment in the low energy region seems to be possible if a method can be found for raising the valence bands L_3' at L. The question of the proper ordering of the energy bands at Γ will have to remain open until further experiments are done.

Acknowledgements

We would like to thank Mr. Frank Serduke for the numerical integration routine used in evaluating the non-local matrix elements (12), and Mr. John Walter for the program used in calculating $R(\omega)$ as well as the quadratic interpolation routine used in evaluating $\varepsilon_2(\omega)$. We would also like to extend our thanks to Professor T. K. Bergstresser and Dr. J. C. Phillips for many helpful discussions and to Professor W. C. Walker for sending us enlarged copies of the $\varepsilon_2(\omega)$ and $R(\omega)$ data used in this paper. One of us (L.A.H.) wishes to express his appreciation to the United States Office of Education for support received under Title IV of the National Defense Education Act during part of the period represented by this calculation. C.Y.F. would like to thank the University of California for a University Fellowship (1969) at the Davis campus. Part of this work was done under the auspices of the United States Atomic Energy Commission.

Bibliography

1. W. Saslow, T.K. Bergstresser, and M. L. Cohen, Phys. Rev. Letters 16, 354 (1966).
2. Van Haeringen, W., and Junginger, H.G., (to be published).
3. L. Saravia and D. Brust, Phys. Rev. 170, 683 (1968).
4. R. Keown, Phys. Rev. 150, 568 (1966), and the references therein.
5. F. Herman, R. L. Kortum, C. D. Kuglin, and R. A. Short, The Physics of Semiconductors (Physical Society of Japan, Kyoto, 1966), p.7.
6. M. L. Cohen and T. K. Bergstresser, Phys. Rev. 141, 789 (1966).
7. J. C. Phillips and L. Kleinman, Phys. Rev. 116, 287 (1959).
8. P. W. Anderson, Concepts in Solids, Benjamin, New York, 1963, p. 66.
9. M.J.G. Lee and L. M. Falicov, Proc. Roy. Soc. A304, 319 (1968).
10. C. Y. Fong and M. L. Cohen, Phys. Rev. 185, 1168 (1969).
11. S. Gotlicher and E. Wölfel, Z. Electrochem 63, 891 (1959).
12. M. Renninger, Acta Cryst. 8, 606 (1955).
13. D. Brust, Phys. Rev. 134, A1337 (1963).
14. W. Saslow, T. K. Bergstresser, C. Y. Fong, and M. L. Cohen, Solid State Communications 5, 667 (1967).
15. J. Walter and M. L. Cohen, Phys. Rev. 183, 763 (1969).
16. R. A. Roberts and W. C. Walker, Phys. Rev. 161, 730 (1967).
17. P. J. Dean, E. C. Lighttowlers, and D. R. Wright, Phys. Rev. 140, A352 (1965).
18. C. D. Clark, P. J. Dean, P. V. Harris, Proc. Roy. Soc. (London) A277, 312 (1964).
19. E. O. Kane, Phys. Rev. 146, 558 (1966).
20. D. M. Roessler, Brit. J. Applied Phys. 16, 1119 (1965).

Table Captions

Table 1: Non-local and local form factors (expressed in Ryd.) used in the present calculation. Also included are the form factors employed in prior EPM calculations

Table 2: Prominent interband transitions, indirect band gap, and positions of the conduction band minimum and main peak in ε_2 for recent diamond calculations, including the present one. Experimental values are included when applicable.

Table 3: Theoretical and experimental ε_2 structure and their identifications including the location in the Brillouin zone, energy, and symmetry of the calculated critical points. The experimental results are due to Roberts and Walker (Ref. 16).

	LOCAL				NON-LOCAL	
	V_{111}	V_{220}	V_{311}	V_{222}	A	α
Present Calculation	-.785	.189	.138	.071	-.159	1.25
Saslow, et.al.[a]	-.811	.337	.132	.041	--	--
Savaria, et.al[b]	-.514	-.022	.186	-.078	--	--
Van Haeringer, et.al.[c]	-.696	.337	.132	0	--	--

[a]Ref. 1

[b]Ref. 2

[c]Ref. 3

Table 1

	Principal Energy Gaps (eV)							
	$\Gamma_{25} \rightarrow \Gamma_{15}$	$\Gamma_{25} \rightarrow \Gamma_2$	$L_3' \rightarrow L_2'$	$L_3' \rightarrow L_3$	$X_4 \rightarrow X_1$	$\Gamma_{25} \rightarrow \Delta_{min}$	Δ_{min}	ϵ_2 Main peak
Present Calculation (Non-local EPM)	8.22	6.96	8.27	13.13	11.79	5.46	.80	11.8 eV
Saravia & Brust[d] (EPM)	14.06	7.52	7.39	17.2	10.43	5.37	.83	~11.0
Herman, et.al.[e] (OPW)	7.1	14	20.5	12.8	11.8	5.47	.75	
Saslow, Bergstresser, Cohen[f] (EPM)	7.33	12.04	10.88	12.8	12.9	5.26	.76	12.7
Van Haeringer, Junginger[g] (EPM)	8.21	12.0		13.0	12.66	5.45	~.8	
Keown[h] (APW)	5.8				11.1			
Experiment	7-7.3*[a,c]	7-7.3*[a,c]			~12	5.47[c]	.78[b]	12[a]

*The entry in this slot depends on whether one assigns the direct gap at Γ to the $\Gamma_{25}' \rightarrow \Gamma_{15}$ or $\Gamma_{25}' \rightarrow \Gamma_2'$ transitions.

[a] Ref. 16
[b] Ref. 17
[c] Ref. 18
[d] Ref. 3
[e] Ref. 5
[f] Ref. 1
[g] Ref. 2
[h] Ref. 4

Table 2

ϵ_2 Structure (eV)		Associated Critical Points		
Theory	Experiment	Location in Zone	Symmetry	CP energy (eV)
8.1	7.2	$\Gamma_{25'} \rightarrow \Gamma_{15}$ (0,0,0)	M_0	8.22
8.3	7.8	$L_{3'} \rightarrow L_2$, (.5,.5,.5)	M_1	8.27
11.8	12.0	$X_4 \rightarrow X_1$ (1,0,0)	M_1	11.79

Table 3

Figure Captions

Fig. 1: Energy bands along principal symmetry lines.

Fig. 2: Calculated and experimental $\epsilon_2(\omega)$ spectra. The full line represents the calculated results using $V_{NL}(\underline{r})$, while the experimental curve is denoted by the dashed line.

Fig. 3: The calculated reflectivity (full line) is compared to the experimental curve (dashed line).

Fig. 4: 4→5 energy contours and critical points in the (a) ΓLK and ΓLUX planes, and (b) ΓKWX plane.

Fig. 5: 4→6 energy contours and critical points in the ΓLK and ΓLUX planes.

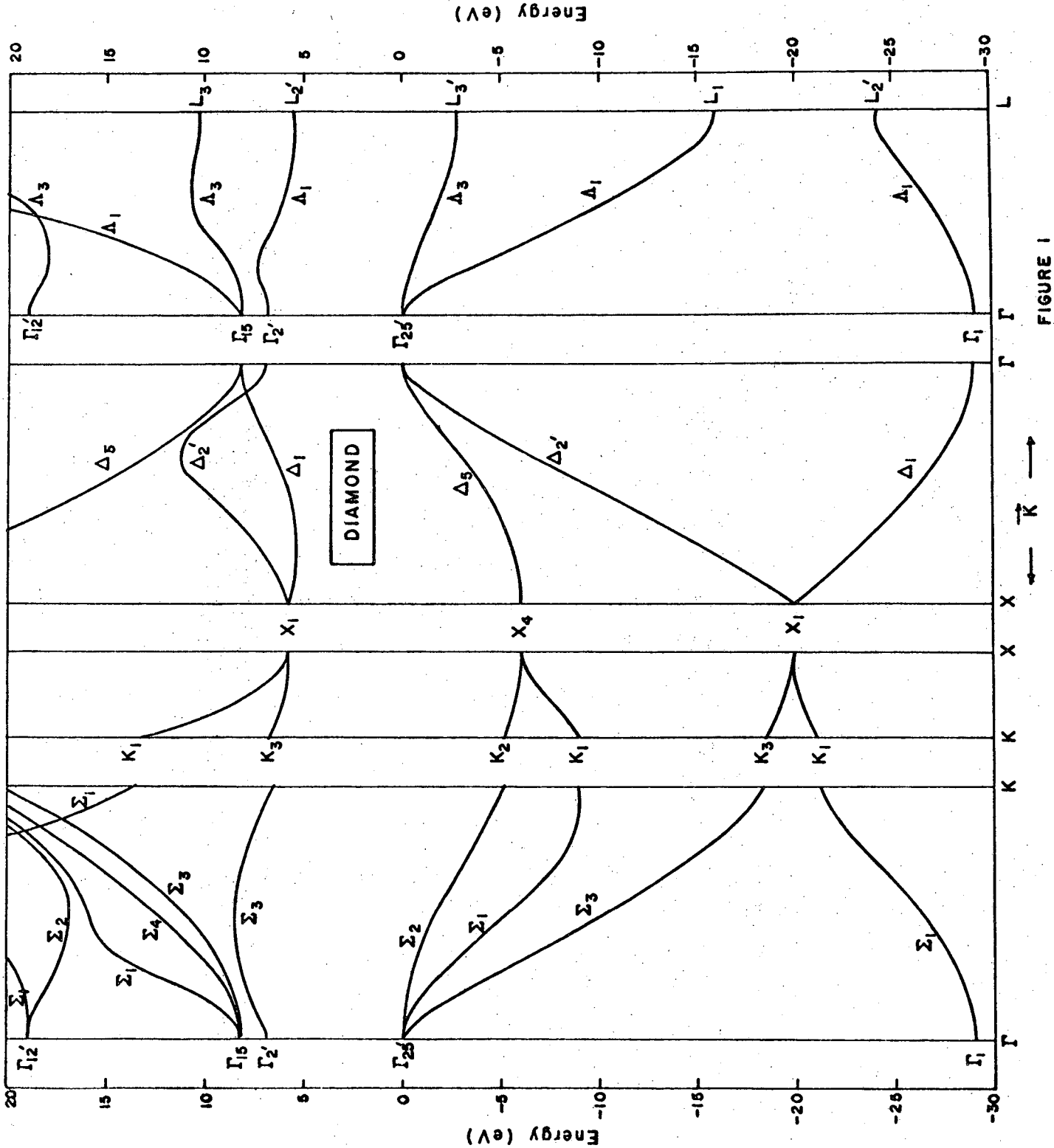
Energy (eV)
20
15
10
5
0
-5
-10
-15
-20
-25
-30
L
Γ
X
K
DIAMOND
$\vec{K}$
L_3
L_2'
L_3'
L_1
L_2'
Λ_3
Λ_1
Γ_{12}'
Γ_{15}
Γ_2'
Γ_{25}
Γ_1
Δ_5
Δ_2'
Δ_1
X_1
X_4
K_1
K_3
K_2
Σ_1
Σ_2
Σ_3
Σ_4

FIGURE 1

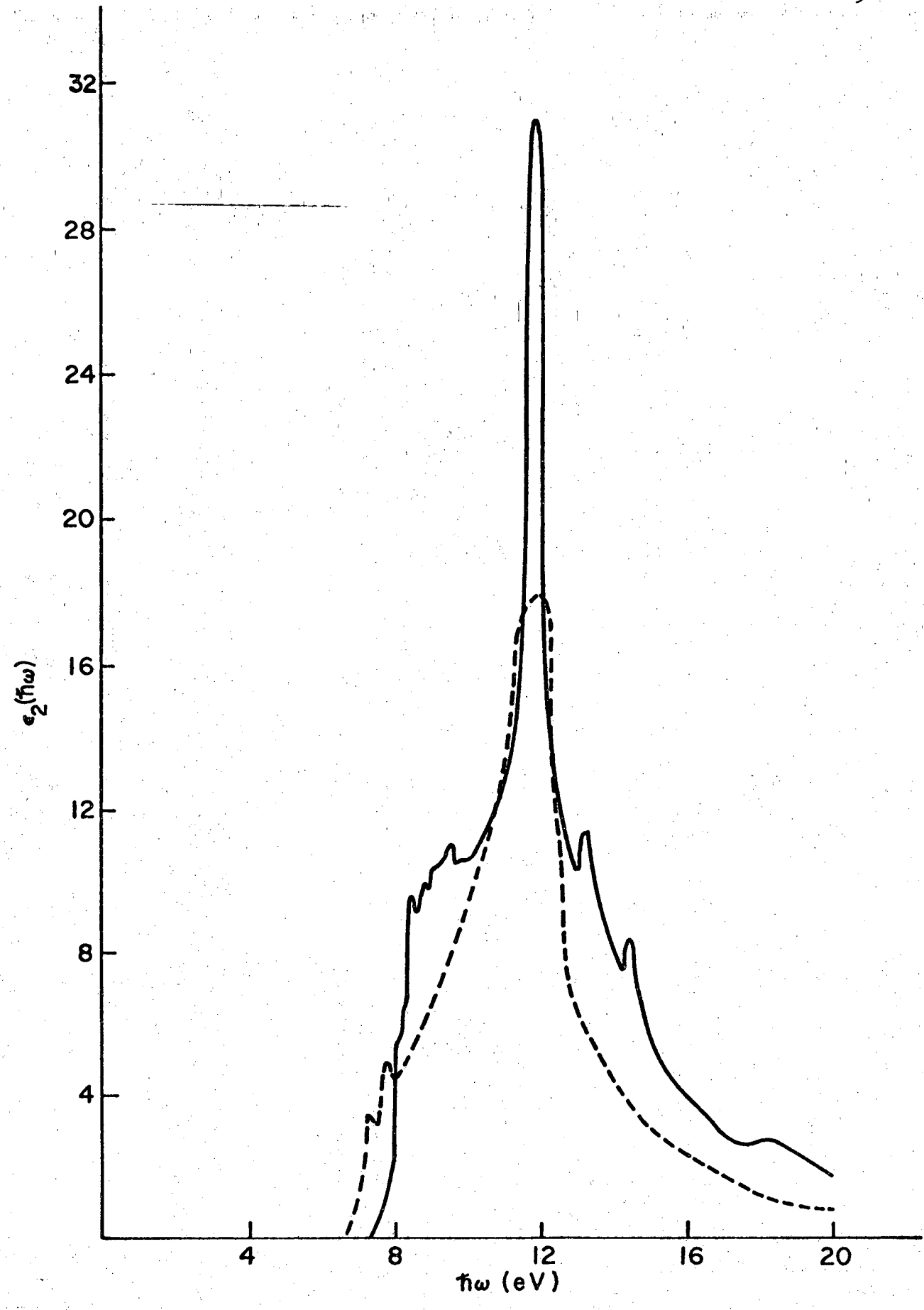
32
28
24
20
16
12
8
4
$\epsilon_2(\hbar\omega)$
2
4
8
12
16
20
$\hbar\omega$ (eV)

FIGURE 2

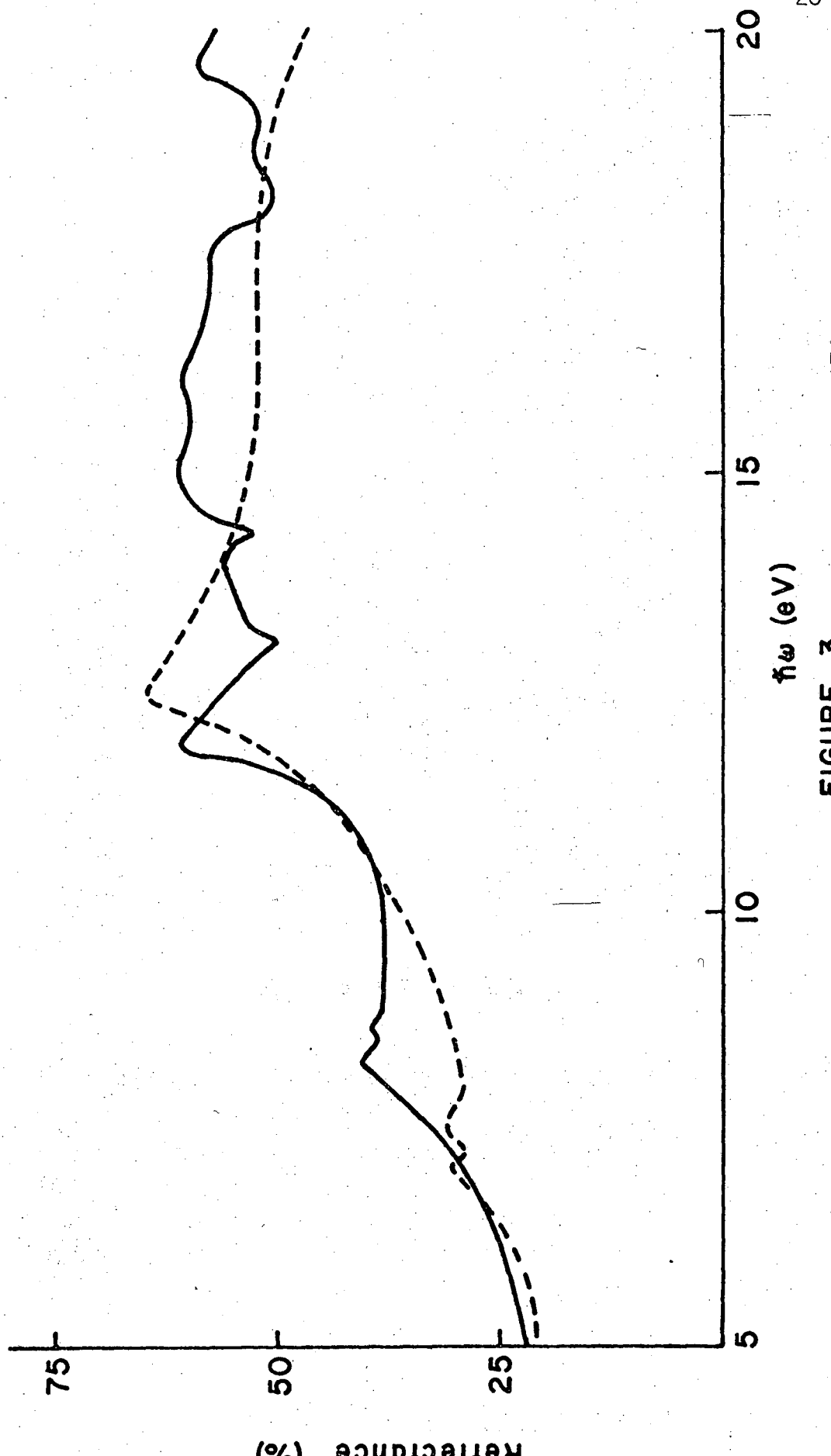

FIGURE 3

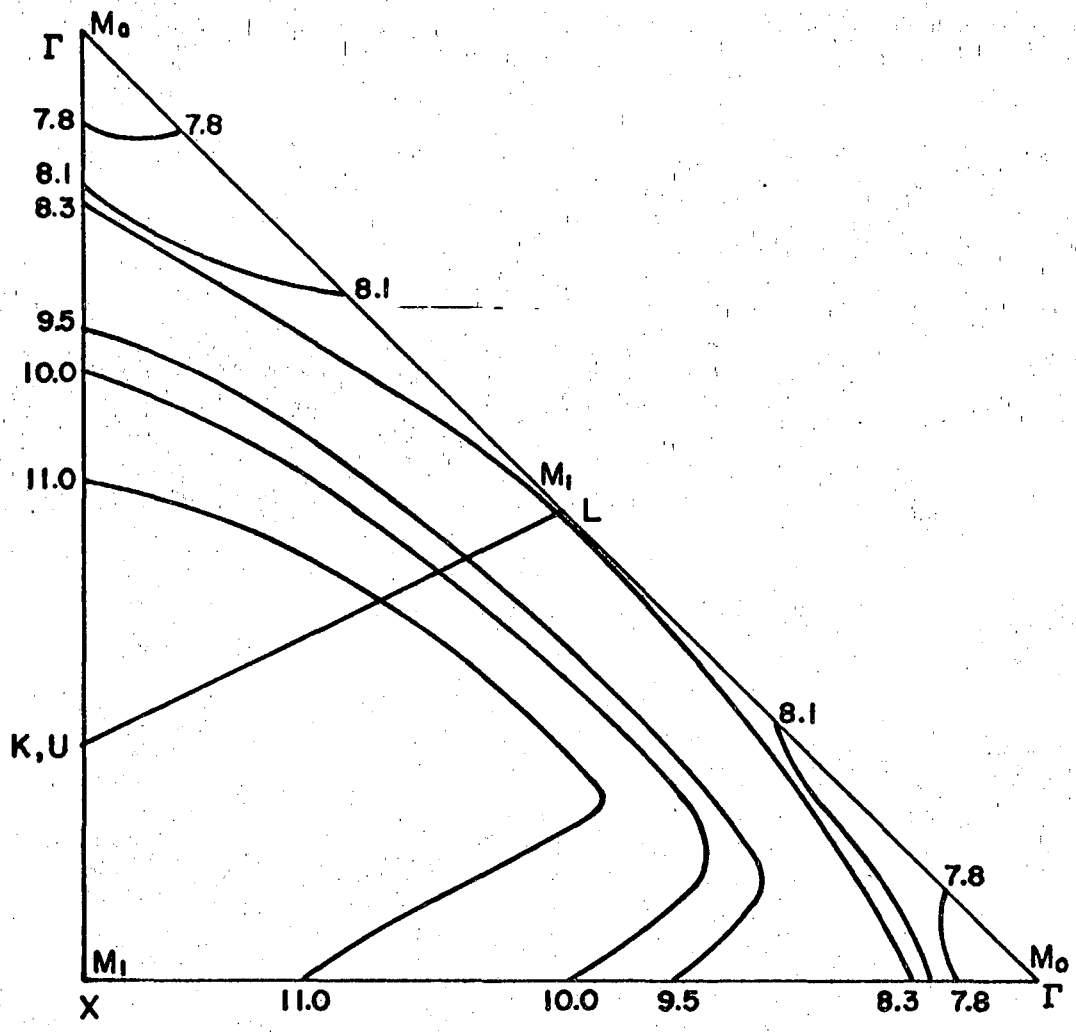
Γ
M₀
7.8
7.8
8.1
8.3
8.1
9.5
10.0
11.0
M₁
L
8.1
K,U
7.8
M₁
M₀
X
11.0
10.0
9.5
8.3
7.8
Γ

(a)

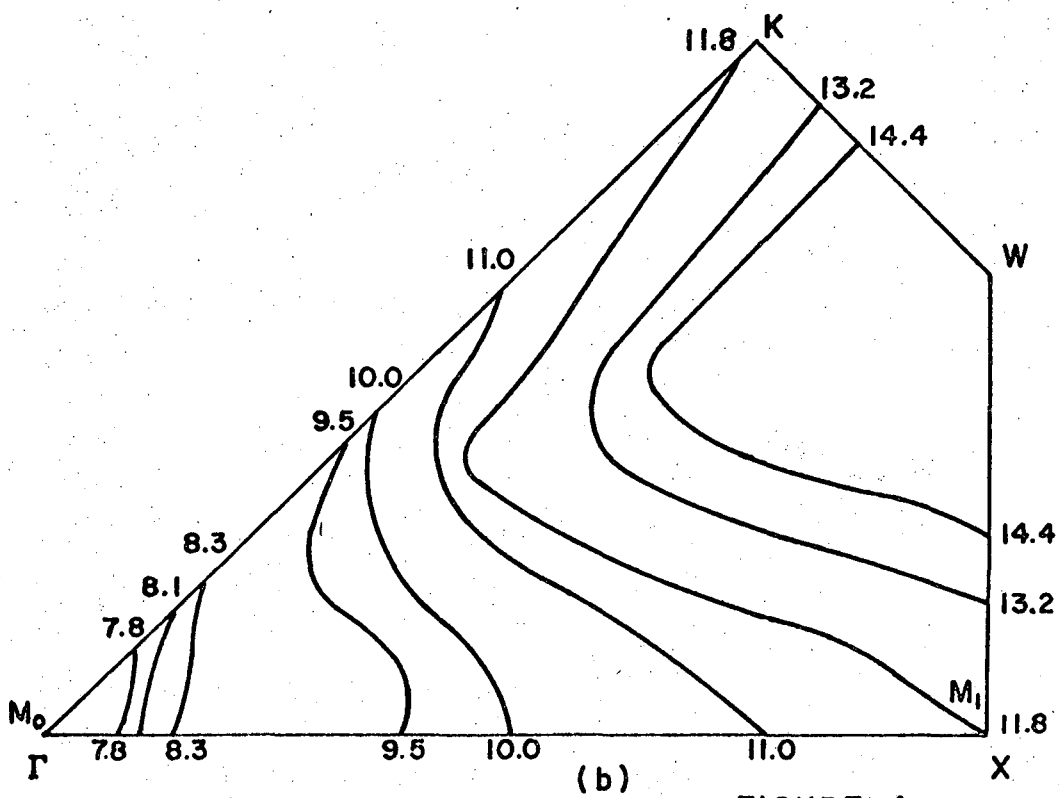
11.8
K
13.2
14.4
11.0
W
10.0
9.5
8.3
8.1
7.8
14.4
13.2
M₁
11.8
M₀
Γ
7.8
8.3
9.5
10.0
11.0
X

(b)

FIGURE 4

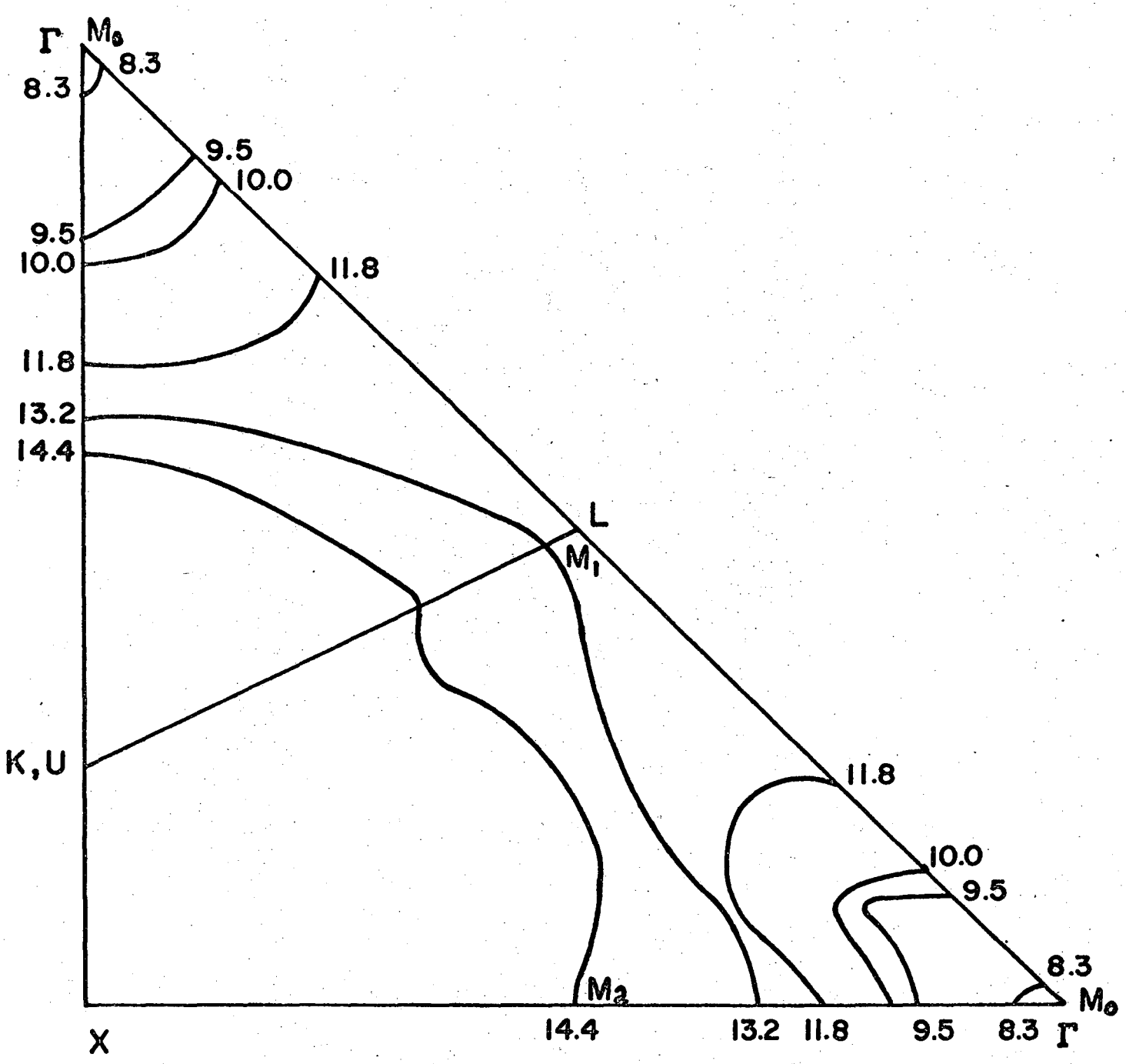
Γ
M₀
8.3
8.3
9.5
10.0
9.5
10.0
11.8
11.8
13.2
14.4
L
M₁
K, U
11.8
10.0
9.5
8.3
M₀
M₂
X
14.4
13.2
11.8
9.5
8.3
Γ

FIGURE 5

LEGAL NOTICE

This report was prepared as an account of Government sponsored work. Neither the United States, nor the Commission, nor any person acting on behalf of the Commission:

A. Makes any warranty or representation, expressed or implied, with respect to the accuracy, completeness, or usefulness of the information contained in this report, or that the use of any information, apparatus, method, or process disclosed in this report may not infringe privately owned rights; or

B. Assumes any liabilities with respect to the use of, or for damages resulting from the use of any information, apparatus, method, or process disclosed in this report.

As used in the above, "person acting on behalf of the Commission" includes any employee or contractor of the Commission, or employee of such contractor, to the extent that such employee or contractor of the Commission, or employee of such contractor prepares, disseminates, or provides access to, any information pursuant to his employment or contract with the Commission, or his employment with such contractor.

TECHNICAL INFORMATION DIVISION
LAWRENCE RADIATION LABORATORY
UNIVERSITY OF CALIFORNIA
BERKELEY, CALIFORNIA 94720